Formation of Mn-skarn Ores at Thapsana Mines, Paros Island, Attico-Cycladic Metallogenetic Massif, Greece

MICHALIS FITROS [1],

STYLIANOS F. TOMBROS[1],

XENOFON C. SIMOS[1],

SOTIRIOS KOKKALAS[1, 2],

KONSTANTIN HATZIPANAGIOTOU[1],

[1]*Department of Geology, University of Patras, Rion, 26500, Patras, Hellas*

[2]*Department of Geosciences, The Petroleum Institute, Khalifa University of Science and Technology, 2533, Abu Dhabi, UAE*

[1]Corresponding author: e-mail tombrosfs@gmail.com.

Μορφοποιήθηκε: Εσοχή: Πρώτη γραμμή: 0"

Abstract

Mn-skarn ore deposits are relatively infrequent worldwide. A typical example of a Mn-skarn in the Attico-Cycladic Metallogenetic Massif is located at the mining area of Thapsana, Paros Island. The skarn occurs adjacent to the Thapsana, highly sericitized, biotite-garnet-tourmaline-lepidolite leucogranite apophyses of the Paros granitoid and related pegmatites and aplites The Mn-skarns orebodies occur as lenses and NE-trending veins hosted in the Cyclades Blueschist Unit (CBU) marbles and intercalated calcic schists. They comprise two discontinuous paragenetic zones (with widths of ≤ 10 m): A zone that contains vesuvianite, Mn-enriched salite to johannsenite-diopside and spessartine with cores enriched in grossular component ($Sps_{\sim 75}Grs_{\sim 15}$), placed close to the Thapsana leucogranite, and a zone of grossular ($Sps_{\sim 85}Grs_{\sim 5}$), actinolite to Mn-cummingtonite (with Mn ~ 0.6 apfu) and phlogopite more distal from the leucogranite. The Mn-skarns are crosscut by later WNW- to W-trending veins filled with Ca-K-Mg-bearing pyrolusite, manganite, rhodonite and rhodochrosite, carbonates, hydroxylapatite and johnbaumite.

The Mn-ores occur as massive aggregates or disseminated comprising jacobsite, hausmannite, Mn- enriched magnetite, braunite and hollandite (with crystals of ≤ 4cm). Occasionally jacobsite and hausmanite display oriented intergrowths. The ore paragenesis also includes secondary pyrolusite, manganite, rhodonite, rhodochrosite, cryptomelane, manjiroite, vernadite and supergene Fe-oxides. Geothermo-oxygen-barometry suggests that the main zones of the Mn-skarns at Thapsana have been formed at temperatures ranging from ~ 440º to ~ 510ºC, pressures of 0.11 to 0.12 GPa. Almost constant average isotopic compositions obtained from the Mn-ores (n = 10) of $\delta^{44}Ca_{BSE}$ and $\delta^{26}Mg_{DSM\text{-}3}$ of 0.5 ± 0.05 and -0.6 ± 0.1 and $\delta^{18}O$ and δD of 7.2 ± 0.5 and -92 ± 2 per mil, suggest a magmatic source for the metasomatic ore fluids related to the Thapsana leucogranite which have also interacted and isotopically equilibrated with the host CBU marbles.

Keywords: Mn-skarn, jacobsite-hausmannite, spessartine, Thapsana, Paros, Cyclades.

Introduction

Skarns are commonly classified, as magnesian, calcic, and mangan based on dominant composition of their protolith and resulted skarn paragenesis [1]. Mangan skarn and related ore deposits are relatively infrequent worldwide (e.g., Groundhog New Mexico, USA [2]; Nakatatsu, Japan, [3]; Yoenhwa-Ulchin, S. Korea, [4]; Gasborn, West Bergslagen, Sweden [5]; Bajiazi Zn-Pb-Ag, Liaoning, China [6]), and yet poorly studied. The Mn-skarns display some distinctive features in mineralogy, zoning patterns, manifestation, and related-ore deposits, which distinguish them from the magnesian and calcic ones. The distinguishing features of the mangan skarns include an unusual Mn-enriched assemblage [7], comprising Mn-olivine (e.g., tephroite), -pyroxene (e.g., johannsenite, Mn-salite, and -hedenbergite) and -pyroxenoid (e.g., rhodonite, bustamite, pyroxmagnite Mn-wollastonite and -babingtonite), -ilvaite and -vesuvianite and -garnet (e.g., spessartine). The retrograde assemblage composes of Mn-amphibole (e.g., Mn-actinolite and cummingtonite), Mn-epidote and piemontite and rhodochrosite. Spatial zoning patterns comprise proximal spessartine, distal johannsenite and Mn-hedenbergite and Mn-vesuvianite and -pyroxenoids sited at the skarn-marble contacts [7]. The Mn-skarns commonly occur along the lithological contacts of their host rocks, i.e., dolomites, marbles and limestones, shales and quartzites as metasomatic veins, lenses or pipes or along faults or fractures, and associate to diorites, monzonites, granodiorites, granites, and in some cases quartz porphyries. They usually are infiltrational, and form between 200º to 400ºC, later than the calcic skarns and occasionally overprint them. The Mn-skarns are typically accompanied by Pb-Zn (± Ag-Cu) ore deposits [1-4].

An illustrative example of a Mn-skarn is placed in the Attico-Cycladic Metallogenetic Massif, Greece, and exposed at the mining area of Thapsana, Paros Island. The Thapsana Mn-skarn is unusual as occurs adjusted to the homonymous spessartine-tourmaline-biotite-lepidolite leucogranite apophyses of the Paros granitoid and related pegmatites and aplites. Herein, we report the results of a comprehensive study of the geological, mineralogical, paragenetic and thermodynamic estimations of the Mn-skarns and stable isotopic compositions

of the ore minerals (e.g., $\delta^{18}O$, δD, $\delta^{44}Ca$, $\delta^{26}Mg$). We have used this information to constrain the physicochemical conditions of the Thapsana skarn and ore formation.

Geological setting of Cyclades and Paros Island

The Attico-Cycladic Metallogenetic Massif (ACM) has a complex geological, magmatic and tectono-metamorphic history that documents the closure of a Neotethyan ocean basin and associated subduction and collision during the Cenozoic. The latter resulted from the convergence between the Apulian microplate and the Eurasian continent from Jurassic until Miocene [8]. Later, an extensional tectonic setting associated with southward retreat of the Hellenic subduction zone and westward extrusion of the Anatolian plate contributed to the final exhumation and exposure of the ACM rocks at the surface [9].

From the lowermost to the upper structural levels the ACM (Fig. 1) consist of: (i). The Basement Unit (BU) (equivalent to the lowermost part of *Marathi nappe* of [10]) composed of Hercynian ortho- and para-gneisses, schists and amphibolites [11] that are exposed as metamorphic core complexes (MCC [12]), (ii). The overlying Cycladic Blueschist Unit (CBU) represents a succession of a late Paleozoic-Mesozoic continental margin, which comprises a Pre-Alpidic anatectic basement overlain by a volcano-sedimentary sequence [13]. The CBU displays a complex metamorphic evolution. It was subjected to high pressure-low temperature (HP-LT) burial conditions during the blueschist to eclogite facies (M1) metamorphism ($T \approx 450°$ to 550°C and $P \approx 15$-20 kbar [8,14]) associated with collisional processes involving Apulia and Eurasia, at ~ 55-40 Ma. This event was followed by a regional Barrovian-type (M2a) metamorphic overprint, between 23-16 Ma [15]. In the central part of Cyclades, the basement gneisses were locally migmatized (M2b event) at upper amphibolite facies (e.g., Naxos and Paros domes), as a result of isothermal decompression exhumation and MCC extension at $T \approx 670° \pm 50$°C and $P \approx 5$-7 kbar ([16] and reference therein). The CBU in Paros comprise a series of tectonically intercalated marbles, amphibolites and mica-schists (formerly known as the *uppermost Marathi nappe* [11]). On Paros the Miocene Barrovian-style metamorphism has pervasively overprinted any earlier HP signature [11].

Above the CBU and below the Upper Cycladic unit (UCU), there is a very low-grade unit of possibly Permian age that consists of marbles, phyllites and metabasic rocks (formerly the

Dryos nappe of [10]). A low angle detachment separates the MCC footwall block from the hanging-wall UCU (formerly the *Marmara nappe* of [10]). The structurally higher UCU is a poorly preserved heterogeneous sequence that locally overlies the CBU. It mainly comprises Permian to Mesozoic marbles, dismembered ophiolites and Late Cretaceous greenschist-to-amphibolite facies rocks that show no evidence of high pressure metamorphic conditions [17]. The tectonic juxtaposition of UCU with the underlying CBU was possibly accomplished in early Miocene [18]. The UCU sediments on Paros are mainly exposed on the eastern part of the island and consist of a gently folded, incomplete marine sequence overlain by a polymictic conglomerate interbedded with sandstones of variable grain size and bed thickness. These lower clastic sedimentary rocks are topped by flat-lying limestone and travertine deposits of possible Pliocene age [19].

The Paros and Thapsana leucogranites and contact aureole

In the mid-to late Miocene, the magmatic arc migrated to the south producing syn- to post-extensional granitoids that cut the regional foliation and in some cases are deformed by the extensional detachments [20]. However, in few cases granitoids ascent and emplace under a transitional setting from transpression to extension [21]. The Miocene granitic intrusions of Paros occur as small ellipsoid laccoliths, pipes and apophyses in the areas of Kolymbithres, Kamares, Paroikia, Taxiarxes, Logovathra (at the northern part of Paros), Thapsana and Trypiti (at the central and southern parts of Paros) (Fig. 1). These intrusive bodies are classified as monzogranites-to-granites and leucogranites, appear highly porphyritic and intense sericitized and propylitized and contain dioritic enclaves [22, 23]. They have been dated at 11.5-12.4 ± 0.2 Ma (K-Ar biotite and muscovite [11]) and 17.1 Ma (K-Ar and Rb-Sr biotite and muscovite [11]), respectively. The Kolymbithres leucogranite was dated by [24] at 15.5 ± 0.3 to 15.7 ± 0.2 Ma ($^{238}U/^{206}Pb$ on zircon).

The Paros leucogranites compose of quartz, orthoclase and microcline, oligoclase to andesine, allanite, zircon, Mg-hornblende, biotite and magnetite [23]. The peraluminous character of the Paros leucogranite is also reflected in its accessory mineralogy containing sillimanite, tourmaline, Li-rich muscovite and lepidolite, apatite and garnet [23]. The Paros leucogranite is enriched in volatiles (e.g., B, F), contains ~ 7 wt. % H_2O and has emplaced at pressures of 1.4 to 4.1 kbars and temperatures of ~ 660° to ~ 760°C ([23] and references therein). The Leykes leucogranite contains mega-crystals of alkali feldspars and the Thapsana

Μορφοποιήθηκε: Όχι Επισήμανση

Μορφοποιήθηκε: Όχι Επισήμανση

leucogranitic apophysis spessartine. All the leucogranites are crosscut by pegmatites and aplites which also intrude the BU and CBU and contain of spessartine and tourmaline [25].

The intrusion of Paros leucogranites has caused an extensive contact aureole (≤ 500m [10]) over the adjacent metamorphic rocks of BU and CBU. The hornfelses proximal to the leucogranitic intrusions with metabauxite protoliths comprise the assemblage sillimanite-kyanite-staurolite-corundum whereas those with metabasite protoliths scapolite-diopside-garnet. More distal from the intrusions hornblende and biotite hornfelses are formed over the metapelites of the CBU [10].

The Thapsana Mn-skarns

Local geology

At the abandoned mines of Thapsana, with reserves of ~ 1Mt, mining activity took place during the period of 1950-1965 by Giannoukos Co, with an annual production of ≈ 2500 t. The skarns outcorp at the migmatized gneisses of the BU and cataclastic marbles that intercalate with the calcic schists, amphibolites and hornfelses of the CBU. The Thapsana biotite-muscovite leucogranite which occurs as an apophysis, mostly intrudes in the CBU marbles and amphibolites along an N- to NNE-trending zone that is also crosscut by pegmatite and aplite dikes. In this zone the skarns are more frequent. The skarn orebodies occur as NE-trending veins, lenses and layers that follow the foliation of their host CBU rocks.

The Mn-ores occur as massive aggregates or even disseminated, enclosed in the skarns. Macroscopically, they comprise magnetite, braunite ($Mn^{2+}Mn^{3+}{}_6SiO_{12}$) and hausmanite ($Mn_3O_4$) with crystals of ≤ 4cm, and are accompanied by quartz-phlogopite-albite-epidote. The skarn orebodies and related Mn-ores are crosscut by E- and WNW-trending veins (with widths ≤ 1.5 m) filled with manganite, ankerite, rhodochrosite and pyrite and supergene pyrolusite and goethite.

Petrography

In the Thapsana area, microscopically, three metasomatic zones were recognized based on spatial and textural relations of Mn-spinels, -pyroxenoids, -pyroxenes, -garnets, and -amphiboles. The first zone (with widths of ≤ 10 m) is placed close to the Thapsana leucogranite and contains subhedral johannsenite and euhedral spessartine with crystals of ≤ 2 cm (Jhn-Sps zone). This assemblage that occurs as massive aggregates or disseminated, relates to stage I of

the Mn-mineralization, i.e., jacobsite, hausmannite, magnetite and braunite. The oxides hausmannite and jacobsite occur as ≤ 2 cm, rounded crystals in intergrowths with each other and with clinopyroxenes and garnets or sometimes replacing the silicate minerals.

More distal from the Thapsana leucogranite, the second metasomatic zone (≤ 20 m wide) comprises fine-grained spessartine, hornblende, cummingtonite and phlogopite replacing the minerals of the johannsenite and spessartine zone (Sps-Cum zone). Phlogopite replaces the amphiboles and garnets with distinctive kink-bands texture. This zone relates to the secondary Mn-mineralization, i.e., stage II that occurs as massive aggregates of hollandite, pyrolusite, manganite, cryptomelane, manjiroite, vernadite and supergene Fe-oxides. Stage II Mn-ore minerals mainly deposit as stockwork veins with open space filling and boxwork textures. The third metasomatic zone (of ≤ 5m in width) is barren, occurs adjusted to the marbles and calcic schists and composes of rhodonite and subordinate vesuvianite.

Analytical methods

The mineralogical and textural characteristics of the samples were studied in polished-thin sections in polarizing optical and scanning electron microscopes (SEM). Mineral microanalyses were performed using a JEOL JSM-6300 SEM equipped with energy dispersive and wavelength spectrometers (EDS and WDS) and INCA software at the Laboratory of Electron Microscopy and Microanalysis, University of Patras, Greece. Operating conditions were accelerating voltage 25 kV and beam current 3.3 nA, with a 4-m beam diameter. The total counting time was 60 s and dead-time 40%. Synthetic oxides and natural minerals were utilized as analytical standards. Detection limits are ~ 0.01% and accuracy better ≥ 5% was obtained.

Materials of 500-mg splits for stable isotope studies were obtained from the coarse-grained Mn-oxides, i.e., jacobsite, hausmannite, magnetite and braunite from the johannsenite-spessartine zone. All minerals selected were handpicked and checked under a binocular microscope to ensure a purity of > 95%. Isotopic compositions of oxygen and hydrogen analyzed using a MAT-253 stable isotope ratio mass spectrometer. All of our isotopic analyses were performed at the Beijing Research Institute of Uranium Geology, China National Nuclear Corporation (CNNC), the Modern Analysis Center, Nanjing University, Nanjing, China as well as, the Chinese Academy of Geological Sciences (CAGS), Beijing, China. Oxygen and hydrogen were released using the BrF_5 extraction technique of [26]. Hydrogen was released from fluid inclusions in the Mn-oxide grains (with a weight of approximate 2 g) by thermal

decrepitation. The samples were pre-heated up to 200 °C, and then re-heated ≥ 500 °C, and reacted with zinc powder at ~ 400 °C to generate hydrogen, and by this treatment we have largely eliminated the effects of the secondary fluid inclusions to the hydrogen isotope composition as the majority of them were decrepitated. Analytical precision was better than ± 0.2 ‰ for $\delta^{18}O$ and ± 2 ‰ for δD.

Ca and Mg isotope analyses were performed in the Mn-oxides from the johannsenite-spessartine skarn zone, using a Thermo-Fisher Triton multicollector thermal ionization mass spectrometer, following the method of [27]. Measurements were made yielding a ^{44}Ca beam intensity that was typically between 3.5 and 4.0 V. Mass 43.5 was measured, which records doubly charged ^{87}Sr, to correct for Sr interference. Every sample is bracketed by measurements of an in-house high-purity ICP Ca standard (HPS). Typical uncertainties $^{44}Ca/^{42}Ca$, $^{44}Ca/^{43}Ca$ and $^{43}Ca/^{42}Ca$ ratios range between 0.01 and 0.02 per mil (all errors are reported at $\pm$ 1 σ), ($^{40}Ca/^{44}Ca$ = 47.162 and $^{42}Ca/^{44}Ca$ = 0.31221). Similar to Ca, precision of Mg isotope measurements is assessed also by synthetic dolomite standard. For both the Ca and Mg isotopes the analytical accuracy was better than ± 0.01 per mil. Reproducibility for $\delta^{44/42}Ca$ was 0.09 per mil (2σ) and $\delta^{44/40}Ca$ values are reported relative to Bulk Silicate Earth (BSE), and for $\delta^{26}Mg$ was 0.1 per mil (2σ) relative to DSM-3 (Deep Sea Magnesium).

Skarn and ore mineral chemistry

Garnet

Garnet is by far the most abundant skarn mineral at Thapsana Mn-skarn. They appear both at the johannsenite-spessartine (Jhn-Sps) and spessartine-cummingtonite (Sps-Cum) zones. Garnet formulae have been calculated normalized on 12 oxygens and 8 cations, based on the formula $X_3Y_2Z_3O_{12}$ (X = Ca^{2+}, Mn^{2+}, Fe^{2+}, Mg^{2+}, Na^{1+}, Y = Al^{IV}, Fe^{3+}, Ti and Cr^{3+}, and Z = Si and Al^{VI}, where X > Y, with Fe^{2+}/Fe^{3+} calculated assuming full site occupancy, and for high Cr and Mn contents MnO corrected for Cr interference). For our calculations we have used the excel sheet GNTCALC provided by GabbroSoft. Garnets from the Jhn-Sps and Sps-Cum zones are isotropic and homogeneous from cores to rims, and appear in equilibrium with johannsenite and cummingtonite. They contain Si = 3.1, Mn ranging from 2.1 to 2.3 and have low Fe^{3+} (≤ 0.2) and Ca (≤ 0.5) values (all in apfu). Their composition is almost pure spessartine ($Sps_{\sim 80 \text{ to } 85}$), with minor andradite component ($Adr_{\sim \leq 10}$) for the Jhn-Sps zone, and almost pure spessartine ($Sps_{\sim 75 \text{ to } 80}$), with minor grossular component ($Grs_{\sim \leq 15}$) for the Sps-Cum zone.

Clinopyroxene and pyroxenoids

Clinopyroxenes from the Jhn-Sps zone are coarse-grained and euhedral with characteristic greenish pleochroism. Usually crystals are highly altered and replaced, particularly around their peripheries and along cleavage planes by hornblende. Pyroxene formulae have been calculated normalized on 6 oxygens, based on the formula $M_2M_1Z_2O_6$ (M_2 = Na, Ca, Fe^{2+}, Mn and Mg, M_1 = Mn, Fe^{2+}, Fe^{3+}, Mg, Cr, Al^{IV}, and Ti and Z = Si and Al^{VI}, where $M_2>M_1$). These clinopyroxenes are zoned and their cores and rims contain Si ranging from 1.8 to 2.0 (all in apfu). Their cores comprise Mn ranging from 0.91 to 0.95 and low Mg ($\leq$ 0.07) and Ca ($\leq$ 0.09), whereas their rims compose of Mn ranging from 0.86 to 0.90, higher Mg ($\leq$ 0.13 to 0.17) and Ca (0.05 to 0.15), respectively (all in apfu). The clinopyroxenes from the Jhn-Sps zone are classified as almost pure Johannsenite ($Jhn_{\sim 80 \text{ to } 90}Di_{\sim \leq 13}$) at their cores, and Johannsenite-Diopside solid solutions ($Jhn_{\sim 60 \text{ to } 70}Di_{\sim \leq 30}$).

Rhodonite occurs in massive aggregates or fills in joints with tabular elongated crystals (up to ~ 1 cm in diameter) of perfect cleavage parallel to the elongation. It intergrowths with fine-grained vesuvianite. Rhodonite formula has been calculated normalized on 3 oxygens, based on the formula MXO_3 (M = Mg, Ca, and Mn, X = Si, Al^{IV}, C, Ge and B). The rhodonite crystals have an almost monotonous composition and contain Si, Fe_{total} Mg, Ca and Mn of ~ 10.1, 0.1, 0.9, 1.2 and 7.4, respectively (all in apfu).

Amphiboles

The amphiboles from the Sps-Cum zone form hypidiomorphic crystals showing intensive pleochroism in shades of green. Their formulae have been calculated normalized on 23 oxygens, based on the formula $A_{0\text{-}1}X_2Y_5Z_8O_{22}(OH)_2$ (A and X = Na, Ca, and K, Y = Al^{VI}, Ti, Cr, Mn, Fe^{2+}, Fe^{3+}, and Mg, and Z = Si and Al^{IV}). The analyzed amphiboles related to Thapsana Mn-skarn are classified as magnesio-mangani- hornblende passing towards cummingtonite (as they have Si-Ca+Li=15, Si-Mg+Li=13 and Si–Na=15). Their Si_{total} and Mg# values range from 6.9 to 7.6 and 3.6 to 4.3 respectively. Additionally their Al_{total} values range from 0.84 to 1.24.

Geo-thermo-barometry

For the estimation of pressure of the Thapsana Mn-skarns we have employed the Al-in-hornblende geobarometer of [28]. In the magmatic hornblendes the Al^{tot} content correlates

linearly with crystallization pressure. The Al-in-hornblende geobarometer was re-evaluated by [29, 30]. The analyzed amphiboles have Al_{total} values that range from 0.84 to 1.24. We have used the [29] equation as it suits better for skarns (for our calculations we have used the excel sheet Pmeter-Al-in-HbBt). Based on the Al-in-hornblende geobarometer the estimated pressure during the formation of Sps-Cum zone ranged from 0.11 to 0.12 GPa.

Temperature estimates were made using the garnet-clinopyroxene geothermometer of [31] which fits best in skarns. The calcium, magnesium and manganese distribution between clinopyroxene and garnet has been calibrated by [32]. In the present calibration, ferric iron in the garnet has been calculated on a stoichiometric basis assuming Z = Si = 3.0, and recalculating ΣXY = 5.0, with ΣX = (Ca + Mn + Fe^{2+}+ Mg) = 3.0 and ΣY = (Fe^{3+} + Al + Cr) = 2.0. For the co-existing clinopyroxene, which all are Na- and Al-poor, Fe^{2+}/Fe^{3+} has been estimated by assuming no jadeite component. The main limitations of the pyroxene-garnet geothermometer are that the clinopyroxene and garnet crystals are in equilibrium and minimum compositional uncertainties must be considerably greater than 0.01Mg# values of analytical errors.

The X_{Ca}^{Grt}, X_{Mn}^{Grt} and $X_{Mg\#}^{Grt}$ values of spessartine and johannsenite in equilibrium range from 0.51 to 0.52, 0.79 to 0.80, and 0.21 to 0.23 respectively and lnK_D values are 100. Application on the clinopyroxene-garnet geothermometer of Pattison and Newton (1989) re-calibrated by [32] using an average calculated pressure of 0.2 GPa gave temperatures ranging from ~ 440º to ~ 510ºC for the Jhn-Sps zone (average of 501ºC and st.d. of 18.3ºC, for our calculations we have used the GrtCpxThermoV5 excel sheet utilizing the equation of [32]).

Stable isotopes

We have analyzed ten crystals of braunite and hausmanite from the Jhn-Sps zone, for their stable isotopic compositions, i.e., $\delta^{18}O$, δD, $\delta^{44}Ca$, and $\delta^{26}Mg$. The isotopic compositions (n = 10) obtained from the Mn-ores are almost constant with an average of $\delta^{44}Ca_{BSE}$ and $\delta^{26}Mg_{DSM-3}$ of 0.5 ± 0.05 and -0.6 ± 0.1. The $\delta^{18}O$ and δD values of these Mn-oxides are 7.2 ± 0.5 and -92 ± 2 per mil. These values suggest a magmatic source for the metasomatic ore fluids related to the Thapsana leucogranite. The mineralizing fluids have also interacted and isotopically equilibrated with the host CBU marbles, schists and amphibolites.

Conclusions

Our concluding remarks based on the synthesis and analysis of geological, mineralogical, and isotopic data in Thapsana Mn-skarns and ores can be summarized as follows:

- Three metasomatic zones were recognized, a Jhn-Sps zone proximal to the leucogranite, a Sps-Cum zone, more distal and a rhodonite and subordinate vesuvianite adjusted to the CBU marbles.
- Garnet are almost pure spessartine ($Sps_{\sim 80 \text{ to } 85}$), with minor andradite component ($Adr_{\sim \leq 10}$) for the Jhn-Sps zone, and almost pure spessartine ($Sps_{\sim 75 \text{ to } 80}$), with minor grossular component ($Grs_{\sim \leq 15}$) for the Sps-Cum zone. Clinopyroxenes from the Jhn-Sps zone are zoned with almost pure Johannsenite ($Jhn_{\sim 80 \text{ to } 90}Di_{\sim \leq 13}$) at their cores, and Johannsenite-Diopside solid solutions ($Jhn_{\sim 60 \text{ to } 70}Di_{\sim \leq 30}$). Amphiboles from the Sps-Cum zone are classified as magnesio-mangani-hornblende passing towards cummingtonite.
- The minimum estimated pressure during the Mn-skarn formation at Thapsana was from 0.11 to 0.12 GPa, at temperatures ranging from ~ 440º to ~ 510ºC.
- Stable isotopic compositions suggest a magmatic source for the metasomatic ore fluids related to the Thapsana leucogranite. The mineralizing fluids have interacted and isotopically equilibrated with the host CBU marbles, schists and amphibolites.

Acknowledgments: We kindly thank A.K. Seferlis from the Laboratory of Electron Microscopy and Microanalysis, University of Patras for his assistance with the SEM microanalyses.

References

1. Meinert, L.D., Dipple, G., Nicolescu, S., 2005. World skarn deposits. Economic Geology 100th Anniversary Volume, Editors: Hedenquist, W.F., Thompson, J., Richard, F.H., Goldfarb, J., Richards, P.J., Society of Economic Geologists, Inc. Littleton, Colorado, p. 299-336.

2. Meinert, L.D., 1987. Skarn zonation and fluid evolution in the Groundhog mine, Central mining district, New Mexico. Economic Geology, v. 82, p. 523-545.

3. Shimizu, M., and Iiyama, J.T., 1982, Zinc-leads skarn deposits of Nakatatsu mine, central Japan: Economic Geology, v. 77, p. 1000-1012.

4. Yun, S., and Einaudi, T.M. 1982. Zinc-lead skarns of the Yeonhwa-Ulchin District, South Korea. Economic Geology. 77. 1013-1032. 10.2113/gsecongeo.77.4.1013.

5. Damman, H.A., 1989, Mn-silicate skarns from the Gasborn area, West Bergslagen, central Sweden. Mineralogical Magazine, 53, 613-626

6. Zhao, Y., Yongguan, D., Daxin, L., and Chengsi, L., 2003. Geology, mineralogy, geochemistry, and zonation of the Bajiazi dolostone-hosted Zn-Pb-Ag skarn deposit, Liaoning Province, China. Ore Geology Reviews. 23. 153-182. 10.1016/S0169-1368(03)00034-9.

7. Zhao, Y., 1991. Manganoan skarn formation. In Skarns-Their genesis and metallogeny, Barto-Kyriakidis, A., Ed. Theophrastus Publications S.A., Athens, p. 165-180.

8. Xypolias, P., Iliopoulos, I., Chatzaras, V., and Kokkalas, S., 2012, Subduction and exhumation related structures in the Cycladic Blueschists: insights from Evia Island (Aegean region, Greece): Tectonics v. 31, TC2001, doi: 10.1029/2011TC002946.

9. Kokkalas, S., Xypolias, P., Koukouvelas, I., and Doutsos, T., 2006, Postcollisional constructional and extensional deformation in the Aegean region, *in* Post-collisional tectonics and magmatism in the Mediterranean region and Asia, Dilek, Y., and Pavlides, S., eds., Geological Society of America, Special Papers, v. 409, p. 97-123, doi:10.1130/2006.2409(06).

10. Papanikolaou, D., 1980, Contribution to the geology of Aegean Sea: The Island of Paros: Annales Geologiques des Pays Helléniques, v. 30, p. 65-96.

11. Altherr, R., Kreuzer, H., Wendt, I., Lenz, H., Wagner, G.A., Keller, J., Harre, W., and Hohndorf, A., 1982, A late Oligocene/Early Miocene high temperature belt in the Attico-Cycladic crystalline complex (SE Pelagonia, Greece): Geologisches Jahrbuch, v. 23, p. 971-164.

12. Gautier, P., and Brun, J.P., 1994, Crystal-scale geometry and kinematics of late orogenic extension in the central Aegean (Cyclades and Evia Island): Tectonophysics, v. 238, p. 399-424.

13. Jolivet, L., Menant, A., Sternai, P., Rabillard, A., Arbaret, L., Augier, R., Laurent, V., Beaudoin, A., Grasemann, B., Huet, B., Labrousse, L., and Le Pourhiet, L., 2015 The geological signature of a slab tear below the Aegean. Tectonophysics, v. 659, p. 166-182, doi:10.1016/j.tecto.2015.08.004Get.

14. Van Hinsbergen, D.J.J., and Schmid, S.M., 2012 Map view restoration of Aegean-West Anatolian accretion and extension since the Eocene. Tectonics 31, TC5005, doi: 10.1029/2012TC003132.

Αλλαγή κωδικού πεδίου

15. Andriessen, P.A.M., Banga, G., and Helbeda, E.H., 1987, Isotopic age study of Pre-Alpine rocks in the basal units on Naxos, Sikinos and Ios, Greek Cyclades: Geologie en Mijnbouw, v. 66, p. 3-14.

16. Keay, S., Lister, G., and Buick, I., 2001, the timing of partial melting, Barrovian metamorphism and granite intrusion in the Naxos metamorphic core complex, Cyclades, Aegean Sea, Greece: Tectonophysics, v. 342, p. 275-312.

17. Papanikolaou, D., 2009, Timing of tectonic emplacement of the ophiolites and terrane paleogeography in the Hellenides. Lithos 108:262-280, doi:10.1016/j.lithos.2008.08.003.

18. Bröcker, M., and Franz, L., 1998, Rb-Sr isotope studies on Tinos Island (Cyclades, Greece): Additional time constraints for metamorphism, extent of infiltration-controlled overprinting and deformational activity: Geological Magazine, v. 135, p. 369-382.

19. Dermitzakis, M., and Papanikolaou, D., 1980, The molasse of Paros Island, Aegean Sea: Annales Naturhist Museum Wien, v. 83, p. 59-71.

20. Kokkalas, S., and Aydin, A., 2013, is there a link between faulting and magmatism in the south central Aegean Sea? Geological Magazine, v. 150, p. 193-224.

21. Menant, A., Jolivet, L., Tuduri, J., Loiselet, C., Bertrand, G., and Guillou-Frottier, L., 2018, 3D subduction dynamics: A first-order parameter of the transition from copper- to gold-rich deposits in the eastern Mediterranean region. Ore Geology Reviews, 94:118-135, doi: 10.1016/j.oregeorev.2018.01.023.

22. McGrath, A.G., 1999, Structural and geochemical evolution of H-type (Hybrid) granitoids in an extensional metamorphic core complex, Paros, Greece: Unpublished PhD, Univ. of Leicester, 170 p.

23. Kevrekidis E., St. Seymour, K., Tombros, S.F., Zhai, D., Liu, J., and Zouzias, D., 2015. The Agios Georgios argentiferous galena deposit on Antiparos Island, Cyclades, Hellas, and its relationship to the Paros leucogranite: Neues Jahrbuch für Mineralogie Abhandlungen-Journal of Mineralogy and Geochemistry, DOI:10.1127/njma/2015/0283.

24. Bargnesi, E.A., Stockli, D.F., Mancktelow, N., and Soukis, K., 2013, Miocene core complex development and coeval supradetatchment basin of Paros, Greece, insights from (U-Th)/He thermochronometry. Tectonophysics, v. 595-596, p. 165-182.

25. Paraskevopoulos, G., Ottemann, J., and Agiorgitis, G., 1972, Manganese-iron-garnets in pegmatites of Paros Island, Greece: Tschermaks, (in German), v.17, p. 247-249.

26. Friedman, I., and O' Neil, J.R, 1977, Compilation of stable isotope fractionation factors of geochemical interest: U.S. Geological Survey Professional Paper 440-KK, p. 1-12.

27. Husson, J. M., Higgins, J.A., Maloof, A.C., and Schoene, B., 2015, Ca and Mg isotope constraints on the origin of Earth's deepest d13C excursion, Geochim. Cosmochim. Acta, 160, 243-266, doi:10.1016/j.gca.2015.03.012.

28. Pattison DRM, Newton RC (1989) Reversed experimental calibration of the garnet-clinopyroxene Fe-Mg exchange thermometer. Contribution to Mineralogy and Petrology 101:87-103.

29. Hammarstrom, J.M., and Zen, E-An (1986) Aluminum in hornblende: an empirical igneous geobarometer. American Mineralogist, 71, 1297-1313.

30. Johnson M.C., and Rutherford M.J., 1989, Experimental calibration of the aluminum-in-hornblende geobarometer with application to Long Valley caldera (California) volcanic rocks // Geology, 17, 9, 837-841.

31. Schmidt, M.W., 1992, Amphibole composition in tonalite as a function of pressure: An experimental calibration of the AI-in-hornblende barometer. // Contributions to Mineralogy and Petrology, 110, 304-310.

32. Krogh Ravna, E., 2000, the garnet–clinopyroxene Fe2+–Mg geothermometer: an updated calibration, Journal of Metamorphic Geology, v. 18, p. 211–219.

Figure captions

Fig. 1. Simplified map of Paros (modified after Papanikolaou, 1980). In the red box is the Mn-skarn of Thapsana.

Fig. 2. a) A view of the relation of skarn zones with marbles and hornfelses. b) A hand specimen of rich spessartine from Mn-skarn. Representative photomicrographs of SEM-EDS of Mn-ore and silicate minerals and the relations between their (c., d., e., f., Abbreviations: Mn-Cpx: manganoan clinopyroxene of Johannsenite-Diopside series, Cum: Cummingtonite, Sps: Spessartine, Jcb: Jacobsite, Hsm: Hausmannite, Hol: Hollandite). Characteristic photomicrographs of polarising microscope of silicate minerals and the relatives between their.

Table 1. Ore paragenesis and hypogene fill minerals from Mn-skarn deposit, Thapsana, Paros.

Table 2. Electron microprobe analyses of I and II stages (wt. %) from Mn-skarn zones, Thapsana, Paros.

Μορφοποιήθηκε: Διάστιχο: Διπλό

Μορφοποιήθηκε: Γραμματοσειρά: 12 στ.

Μορφοποιήθηκε: Γραμματοσειρά: 12 στ.

Μορφοποιήθηκε: Γραμματοσειρά: 12 στ.

Μορφοποιήθηκε: Γραμματοσειρά: 12 στ.

Μορφοποιήθηκε: Γραμματοσειρά: 12 στ.

Μορφοποιήθηκε: Αγγλικά (Ηνωμένων Πολιτειών)

Μορφοποιήθηκε: Αριστερά, Κανένα, Εσοχή: Πρώτη γραμμή: 0", Διάστιχο: μονό

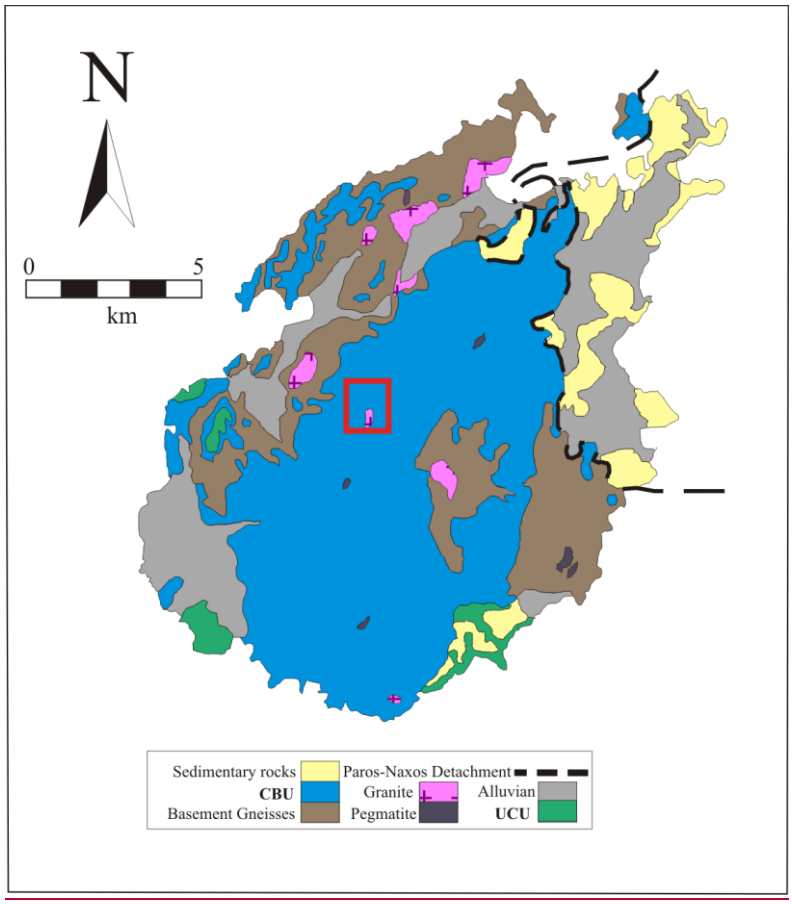

Fig. 1~~Fig. 1. Simplified map of Paros (modified after Papanikolaou, 1980).~~

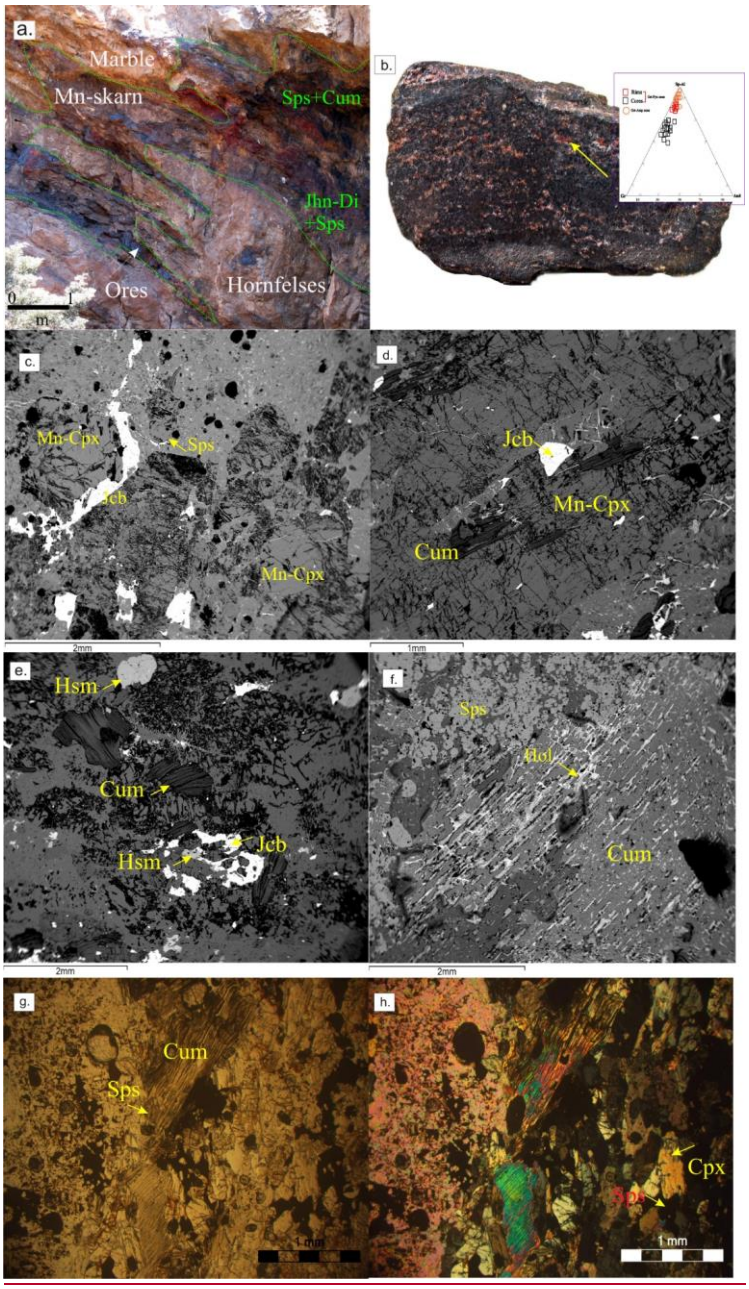
a.
Marble
Mn-skarn
Sps+Cum
Jhn-Di
±Sps
Ores
Hornfelses
0
1
m
b.
c.
Mn-Cpx
Sps
Jcb
Mn-Cpx
2mm
d.
Jcb
Mn-Cpx
Cum
1mm
e.
Hsm
Cum
Jcb
Hsm
2mm
f.
Sps
Hol
Cum
2mm
g.
Cum
Sps
1 mm
h.
Cpx
Sps
1 mm

Fig. 2

Table 1. Ore paragenesis and hypogene fill minerals from Mn-skarn deposit, Thapsana, Paros.

Mineral stages	**Stage I**	**Stage II**
T (°C)	*>500*	*<500-200*
Milky quartz	▬	▬▬▬
Spessartine	▬▬▬▬▬	▬▬▬▬▬
Johannsenite-Diopside	▬▬▬▬	
Mn-Cummingtonite	▬▬	▬▬▬
Phlogopite	▬	▬▬▬
Jacobsite	▬▬▬▬	
Hausmannite	▬▬▬	▬
Hollandite		▬▬▬▬▬
Calcite-Ankerite		▬▬▬
Mn-Magnetite	▬▬	
Hydroxylapatite	▬▬	▬▬
Johnbaumite	▬	▬
Braunite	▬▬	
Manganite		▬▬
Pyrolusite		▬▬▬
Rhodonite	▬▬	▬
Rhodochrosite		▬
Cryptomelane		▬
Manjiroite		▬
Vernadite		▬

Table 2. Electron microprobe analyses of I and II stages (wt. %) from Mn-skarn zones, Thapsana, Paros.

SAMPLE	1	2	3	4	5	6	7	8	9	10
SiO_2	38.84	38.26	53.12	50.22	51.01	40.30	48.01	10.41	0.00	0.19
TiO_2	0.00	0.00	0.00	0.00	0.00	0.67	0.22	0.16	0.00	0.01
Fe_2O_3	1.38	3.22	11.00	0.1	2.43	0.95	0.89	4.23	0.43	67.84
Al_2O_3	19.93	17.77	0.86	15.01	10.86	14.14	0.00	0.63	0.00	6.72
CaO	6.56	4.95	22.74	3.75	13.66	0.51	5.37	1.02	0.00	0.00
MgO	1.67	1.42	0.01	25.07	19.63	26.38	2.72	0.00	0.21	0.44
Mn_2O_3	0.00	0.00	0.00	0.00	0.00	0.00	0.00	0.00	62.7	1.06
MnO	31.61	34.36	11.40	2.84	0.65	0.00	41.21	84.32	32.7	30.07
Na_2O	0.00	0.00	0.25	0.00	0.00	1.00	0.00	0.00	0.00	0.00
K_2O	0.00	0.00	0.00	2.74	0.33	8.80	0.00	0.10	0.00	0.00
Total	99.99	99.98	99.99	99.62	99.97	99.99	99.79	99.98	99.91	99.89
No. of atoms based on										
Si^{total}	3.09	3.09	2.01	6.69	6.94	5.92	2.01	1.00	0.00	0.00
Ti	0.00	0.00	0.00	0.00	0.00	0.31	0.01	0.01	0.00	0.00
Fe^{total}	0.09	0.21	0.35	0.00	0.3	0.44	0.03	0.31	0.01	1.96
Al^{total}	1.87	1.71	0.04	2.30	1.7	2.16	0.00	0.07	0.00	0.07
Mn^{+2}	2.13	2.35	0.64	0.32	0.08	0.00	1.54	5.87	0.1	0.96
Mn^{+3}	0.00	0.00	0.00	0.00	0.00	0.00	0.00	0.00	1.98	0.31
Mg	0.19	0.17	0.01	4.94	3.96	3.77	0.17	0.00	0.02	0.00
Ca	0.56	0.43	0.92	0.53	1.98	0.26	0.24	0.10	0.00	0.10
Na	0.00	0.00	0.02	0.00	0.48	0.46	0.00	0.00	0.00	0.00
K	0.00	0.00	0.00	0.46	0.00	1.99	0.00	0.01	0.00	0.00
O	12.00	12.00	4.00	16.00	16.00	16.00	6.00	12.00	4.00	4.00

	[1] Garnet I [2] Garnet II [3] Pyroxene (Jo-Di) [4] Mn-Cumminghtonite [5] Mg-Hornblend	[6] Phlogopite [7]Rhodonite [8] Braunite [9] Hausmannite [10]Jacobsite

Μορφοποιήθηκε: Αγγλικά (Ηνωμένων Πολιτειών)

Μορφοποιήθηκε: Αριστερά

Μορφοποιημένος πίνακας